Nano Res (2010) 3: 51–60
DOI 10.1007/s12274-010-1008-2
Research Article

Dopant-Controlled Synthesis of Water-Soluble Hexagonal $NaYF_4$ Nanorods with Efficient Upconversion Fluorescence for Multicolor Bioimaging

Xuefeng Yu[1], Min Li[1], Mengyin Xie[1], Liangdong Chen[2], Yan Li[2], and Ququan Wang[1] (✉)

[1] Key Laboratory of Acoustic and Photonic Materials and Devices of Ministry of Education, Wuhan University, Wuhan 430072, China
[2] Department of Oncology, Zhongnan Hospital of Wuhan University, Hubei Key Laboratory of Tumor Biological Behaviors, Wuhan 430071, China

Received: 28 September 2009 / Revised: 25 November 2009 / Accepted: 26 November 2009

ABSTRACT

A novel strategy is proposed to directly synthesize water-soluble hexagonal $NaYF_4$ nanorods by doping rare-earth ions with large ionic radius (such as La^{3+}, Ce^{3+}, Pr^{3+}, Nd^{3+}, Sm^{3+}, Eu^{3+}, and Gd^{3+}), and the dopant-controlled growth mechanism is studied. Based on the doping effect, we fabricated water-soluble hexagonal $NaYF_4$:(Yb,Er)/La and $NaYF_4$:(Yb,Er)/Ce nanorods, which exhibited much brighter upconversion fluorescence than the corresponding cubic forms. The sizes of the nanorods can be adjusted over a broad range by changing the dopant concentration and reaction time. Furthermore, we successfully demonstrated a novel depth-sensitive multicolor bioimaging for *in vivo* use by employing the as-synthesized $NaYF_4$:(Yb,Er)/La nanorods as probes.

KEYWORDS

Crystal growth, hexagonal $NaYF_4$, nanocrystals, fluorescence, bioimaging

Introduction

During the past decades, one-dimensional nanocrystals (NCs) have attracted great research interest for their unique properties and potential applications in nanoscale optics [1], optoelectronics [2], solar cells [3], and biological detection [4, 5]. Most of these applications make great demands on various parameters of the materials, including phase, shape, size, chemical composition, and surface properties. Hence, there have been extensive efforts focusing on the development of novel synthetic methodologies (e.g., reverse micelle templating, seed-mediated growth, and crystal growth regulated by surfactants) for making various nanorods with desired properties [6–10]. With all these methods, it still remains an open challenge to establish a suitable synthetic methodology for growing high-quality one-dimensional NCs of a given material with simultaneous control over phase, size, and surface properties.

In recent years, monodisperse NCs of rare-earth (RE) compounds, such as oxides [11, 12], phosphates [13], fluorides [14, 15], and vanadates [16] have become a new focus of research, due to their reliable optical properties arising from the 4f electron configuration, and potential applications in optics, optoelectronics, sensors, and biolabels. Of these, the RE fluoride compounds with general formula $NaREF_4$, especially $NaYF_4$, have attracted more and more attention because

Address correspondence to qqwang@whu.edu.cn

they have low phonon energy, and are regarded as excellent host materials for both downconversion and upconversion processes [17–19]. Hexagonal $NaYF_4$ NCs are the most efficient upconversion phosphors known until now, and they provide over an order of magnitude stronger fluorescence than the corresponding cubic form [19, 20]. Such upconversion materials promise to be a new class of biological probes owing to their deep tissue penetration of near-infrared (NIR) radiation, efficient multicolor emissions, and very low toxicity [21–24].

Great efforts have been devoted to phase-controlled synthesis of $NaYF_4$ NCs in special organic surfactants [25–37]. Drastic conditions such as extended annealing time, prolonged reaction time, and high temperature have often been used to overcome the free energy barrier to obtain hexagonal $NaYF_4$ NCs. However, most of the hexagonal $NaYF_4$ NCs synthesized so far were protected by hydrophobic ligands, and thus they were often not water-soluble or biocompatible. Parallel efforts have therefore been focused on the synthesis of water-soluble $NaYF_4$ NCs in order to expand their applications to biological areas. Hydrophilic surfactants such as polyvinylpyrrolidone (PVP) and polyethylenimine (PEI) have successfully been used as chelating agents to give water-soluble $NaYF_4$ NCs with mild surface properties; however, the synthesized NCs were usually cubic phase [38, 39] or a mixture of cubic and hexagonal phases [40]. Because hydrophilic agents usually induce an isotropic growth and suppress the formation of hexagonal anisotropic nanostructures, it is still a great challenge to directly synthesize water-soluble hexagonal $NaYF_4$ NCs with controlled size and the desired optical properties.

On the other hand, the doping technique has been widely used to adjust the crystal structure of RE-based bulk materials, such as strontium–barium niobates [41], titanates [42], oxyorthosilicates [43], orthoborates [44], manganites [45], and intermetallic compounds [46]. In 1991, Blasse et al. observed that 50% La doping could induce a complete trigonal to orthorhombic phase transition in bulk GdF_3 crystals [47]. Very recently, van Veggel et al. found that undoped GdF_3 NCs were formed as a mixture of trigonal and orthorhombic phases, and 15% La doping was sufficient for them to crystallize completely in the trigonal phase [48]. However, the dopant-controlled cubic-to-hexagonal phase transition in the RE fluoride NCs has not been reported so far.

In this paper, we first report a study of the doping effect of RE elements with large ionic radius on the phase and shape of the $NaYF_4$:RE NCs. Then, we propose a dopant-controlled method to directly synthesize water-soluble hexagonal $NaYF_4$:(Yb,Er)/Ce and $NaYF_4$:(Yb,Er)/La nanorods with controllable size and greatly improved upconversion fluorescence for multicolor bioimaging.

1. Experimental

1.1 Synthesis procedure

PEI ($M_W = 10\,000$) and all the lanthanide chlorides were purchased from Sigma-Aldrich. Other reagents were purchased from Sinopharm Chemical Reagent Co., Ltd. All the reagents were used as received without further purification. In a typical procedure, a growth solution was prepared by dissolving $RECl_3$ (RE: one RE element or multiple RE elements with an appropriate molar ratio), and NaCl in water with total RE and Na^+ ionic concentrations of 0.5 mmol. Under vigorous agitation, 15.0 mL of ethanol, 5.0 mL of PEI solution (5.0 wt%), and an appropriate amount of NH_4F (F^-/Na^+ ratio of 5) was added, and the mixture was then transferred to a Teflon lined autoclave and heated at 200 °C for several hours. By changing the dopant concentration and reaction time, the crystallite size of the products could be regulated. After cooling down, the resulting $NaYF_4$:RE NCs were washed with ethanol and water several times, and dried in vacuum.

1.2 Instrumentation

The X-ray powder diffraction (XRD) analyses were performed on a Bruker D8 ADVANCE X-ray diffractometer with Cu $K\alpha_1$ irradiation ($\lambda = 1.5406$ Å). The transmission electron microscopy (TEM) and high-resolution transmission electron microscopy (HRTEM) images were recorded with a JEOL 2010 HT and JEOL 2010 FET transmission electron microscope (operated at 200 kV), respectively. The scanning electron microscopy (SEM) images were

measured with a Hitachi X-650 scanning electron microscope. The Fourier transform infrared (FTIR) spectra were recorded on an Avatar-360 spectrometer. The upconversion emission spectra were obtained using a 975 nm continuous-wave (CW) diode laser and recorded by a spectrometer (Spectrapro 2500i, Acton) with a liquid nitrogen cooled CCD (SPEC-10: 100B, Princeton).

1.3 Bioimaging

The synthesized $NaYF_4$:(Yb,Er)/La nanorods with diameter (d) of 20 nm and length (l) of 50 nm were employed as the fluorescent probes. Firstly, the aqueous dispersion of the $NaYF_4$:(Yb,Er)/La nanorods was centrifuged, and the precipitate was re-dispersed in phosphate-buffered saline (PBS) solution by shaking at 37 °C for ~30 min. The pH value of the solution was ~7.4, and the particle concentration was 1.0 mg/mL. Then, the PBS solution of the nanoparticles was filtered with a 0.4 μm syringe filter, and stored at 37 °C before *in vivo* applications. We noted that the prepared PEI coated $NaYF_4$ nanoparticles were stable in PBS without any flocculation; similar results have been reported previously [23]. Using protocols approved by the Institutional Animal Care and Use Committee of Wuhan University, one 6-week-old nude mouse was placed under anesthesia by injection of 3% nembutal at a dosage of 45 mg/kg for *in vivo* studies. The mouse was injected intramuscularly with 100 μL of $NaYF_4$:(Yb,Er)/La nanorods into one leg. NIR excitation was with a 975 nm CW diode laser, and the image was recorded by using an ordinary camera (EOS40D, Canon) equipped with two 300–750 nm band-pass filters (FSR-KG3, Newport) to reject the scatter from the laser. The excitation light was not focused and the power density at the animal was ~200 mW/cm^2. The image was taken after the injected probes adequately penetrated into the tissues (~10 min post-injection) with an exposure time of 2.0 s.

2. Results and discussion

2.1 RE ionic radius-dependent growth behavior of $NaREF_4$ nanocrystals

We first investigated the influence of RE ionic radius on the phase and shape of the $NaREF_4$ NCs. In the case of RE elements with small ionic radius (r), such as Yb^{3+} (r = 0.86 Å) and Y^{3+} (r = 0.89 Å), the synthesized $NaYbF_4$ and $NaYF_4$ NCs were cubic phase nanospheres. For the RE elements with larger ionic radius, such as Gd^{3+} (r = 0.94 Å) and Nd^{3+} (r = 1.00 Å), the synthesized $NaGdF_4$ and $NaNdF_4$ NCs were hexagonal phase nanorods (see Fig. S-1 in the Electronic Supplementary Material (ESM)). This ionic radius-dependent growth behavior of $NaREF_4$ NCs can be explained from the point of view of the free energy of the system [28, 49]. In general, the hexagonal phase $NaREF_4$ is more thermodynamically stable than the cubic form, and the cubic-to-hexagonal phase transition is a disorder-to-order character which requires sufficient free energy to overcome the activation barrier. Thus, high temperature has often been used to provide enough energy to overcome the energy barrier between the cubic and hexagonal $NaREF_4$ [27, 28, 32]. The ionic radius dependence of the energy barriers for hexagonal $NaREF_4$ has been systematically studied by Yan et al. [28]. In their reaction system, the energy barrier for the RE elements Lu to Dy was found to be higher than those for the RE elements with larger ionic radius (Tb to Sm). Similarly, the $NaREF_4$ growth behavior in our reaction system indicates that the RE elements with larger ionic radius (such as Gd^{3+} and Nd^{3+}) have lower energy barriers to the hexagonal phase products.

2.2 RE-dopant-controlled growth behavior of $NaYF_4$: RE nanocrystals

We further investigated the influence of the RE ionic radius on the phase and shape of the RE doped $NaYF_4$ NCs, which were all synthesized with a reaction time of 24 h. The XRD spectra and TEM images in Figs. 1(a) and 1(b) show that the undoped $NaYF_4$ NCs are cubic nanospheres with diameters of ~50 nm. When Gd was used as dopant with a doping concentration of 10%, the synthesized $NaYF_4$:10% Gd NCs became hexagonal short irregular nanorods with diameters of ~35 nm and lengths of ~70 nm (Figs. 1(a) and 1(c)). More interestingly, when La was used as the dopant, the synthesized $NaYF_4$:10%La NCs became hexagonal long nanorods with diameters of ~150 nm and lengths of ~1100 nm (Figs. 1(a) and 1(d)). Their regular hexagonal cross-section can be observed in the corresponding

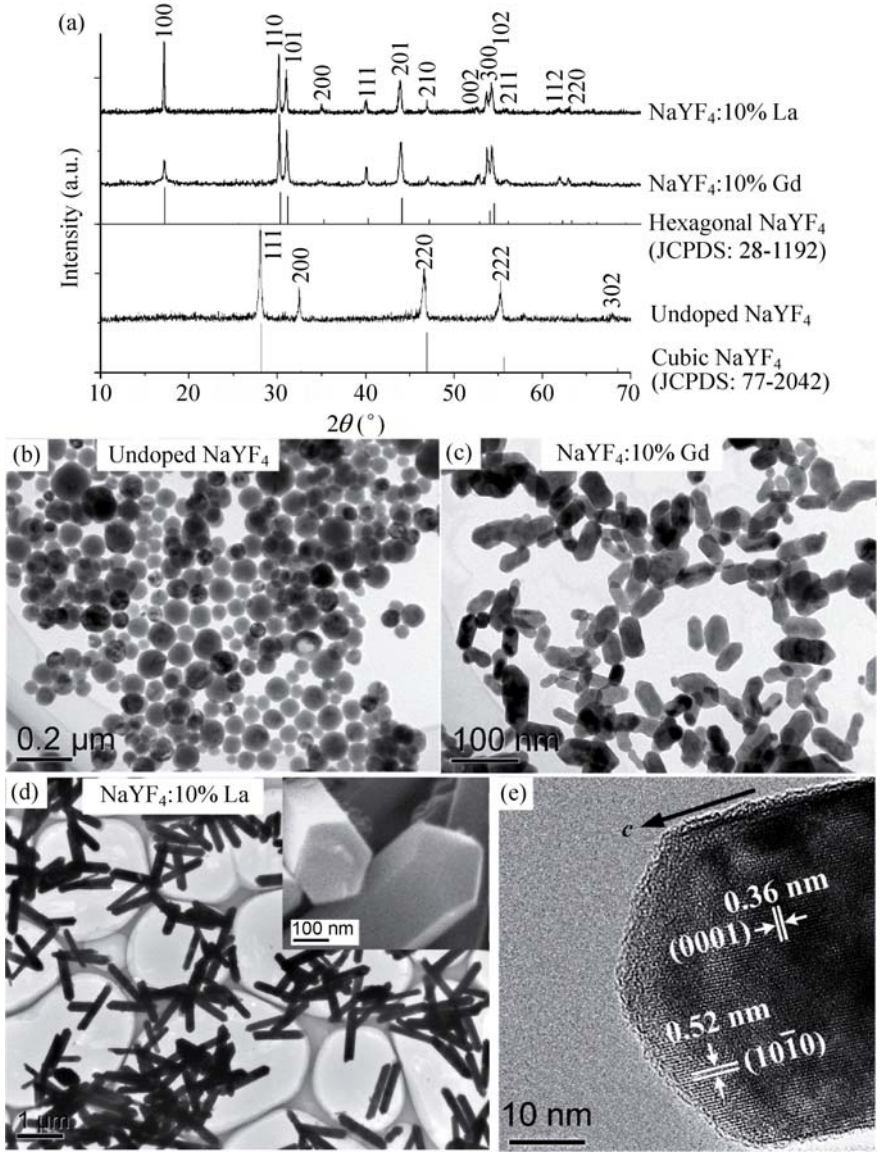

Figure 1 XRD spectra (a) and TEM images ((b)–(d)) of undoped $NaYF_4$, $NaYF_4$:10% Gd, and $NaYF_4$:10% La NCs. The line spectra in (a) correspond to the literature data for cubic $NaYF_4$ (lower spectrum; JCPDS: 77-2042), and hexagonal $NaYF_4$ crystal (upper spectrum; JCPDS: 28-1192). The inset image in (d) shows the SEM image of $NaYF_4$:10% La NCs. (e) HRTEM image of one nanorod. All the samples were synthesized with a reaction time of 24 h

SEM image (inset in Fig. 1(d)). The HRTEM image of one nanorod shown in Fig. 1(e) shows interplanar spacings of 0.52 and 0.36 nm corresponding to the (10–10) and (0001) planes of hexagonal $NaYF_4$, confirming that the nanorods grow along the *c*-axis, namely, the [0001] direction.

Table 1 summarizes the doping effect of the RE elements (from Lu to La, except for Pm) on the phase and shape of the $NaYF_4$:10% RE NCs. It was found that the RE elements could be divided into three groups according to their increasing ionic radius (Ⅰ: Lu, Yb, Tm, Er, Ho, Dy, and Tb; Ⅱ: Gd, Eu, Sm, Nd, and Pr; Ⅲ: Ce and La). The RE dopants in group Ⅰ showed almost no influence on the phase and shape of the $NaYF_4$ host, and thus the corresponding $NaYF_4$: 10% RE NCs were cubic nanospheres with diameters ranging from 45 to 65 nm. In contrast, the RE dopants in groups Ⅱ and Ⅲ could induce the formation of hexagonal $NaYF_4$: 10% RE nanorods. For group Ⅱ, the synthesized $NaYF_4$: 10% RE NCs were irregular short nanorods with lengths ranging from 70 to 110 nm, and their aspect ratios were ~2. For Ce and La in group Ⅲ, the $NaYF_4$:10% Ce and $NaYF_4$: 10% La NCs were regular long nanorods with lengths of up to microns, and their aspect ratios were over 7. The above results indicate that there is a dopant-controlled cubic-to-hexagonal phase transition coupled with a sphere-to-rod shape transformation of the $NaYF_4$:RE NCs (see Fig. S-2 in the ESM for the XRD spectra and TEM images of the $NaYF_4$: 10% RE NCs).

The RE doping effect on the $NaYF_4$ NCs can be ascribed to the system free energy and anisotropic crystal growth. As described above, the RE elements with larger ionic radius give relatively low-energy barriers to the hexagonal phase products in our reaction system. When the doped $NaYF_4$ NCs were synthesized, the RE dopants with larger ionic radius (in groups Ⅱ and Ⅲ) can decrease the energy barrier, and tip the balance in favor of the hexagonal phase during the reaction process. Thus, hexagonal $NaYF_4$

Table 1 The RE doping effect on the phase, shape, and size of the $NaYF_4$:10% RE NCs[a]

Group	RE dopant	Ionic radii of RE^{3+} (Å)	$NaYF_4$:10%RE NCs		
			Phase	Shape	Size range (nm)
Ⅰ	Lu	0.85	Cubic	Nanosphere	$d \approx 45$–65
	Yb	0.86			
	Tm	0.87			
	Er	0.88			
	Ho	0.89			
	Dy	0.91			
	Tb	0.92			
Ⅱ	Gd	0.94	Hexagonal	Nanorod	$l \approx 70$–110 Aspect ratio ≈ 2
	Eu	0.96			
	Sm	0.96			
	Nd	1.00			
	Pr	1.01			
Ⅲ	Ce	1.03	Hexagonal	Nanorod	$l > 1000$ Aspect ratio >7
	La	1.06			

[a] All the samples were synthesized with a reaction time of 24 h. The ionic radius of the Y^{3+} ion is 0.89 Å.

might be formed under appropriate reaction conditions. Such a cubic-to-hexagonal transition process is clearly seen in the XRD spectra of $NaYF_4$:10% Ce NCs with different reaction time (see Fig. S-3 in the ESM). It was found that only cubic phase particles were obtained at the beginning of the reaction at 200 ℃. After 20 min, a small amount of hexagonal phase particles was formed, and almost all the products became the hexagonal phase when the reaction time was over 120 min. In contrast, only cubic products could be obtained at all reaction time if the undoped $NaYF_4$ was synthesized. The results confirm that the dopant-induced phase transition in our reaction system is a gradual process, rather than hexagonal seeds (small particles) being formed at the beginning of the reaction [32]. We noted that other reaction parameters, such as F^-/Na^+ ratio and PEI concentration, could also influence the phase transition and final products. It was found that a small excess of F^- was often needed to induce the complete cubic-to-hexagonal phase transition of the doped $NaYF_4$ NCs. Furthermore, almost no phase transition could be found if PVP was used as the surfactant instead of PEI.

Furthermore, it was found that the RE dopants in group Ⅲ (Ce and La) could efficiently induce anisotropic crystal growth to form long $NaYF_4$ nanorods. Such a doping effect was further investigated by co-doping x% Ce ($x = 4$, 7, 10), 20% Yb, and 5% Er in the $NaYF_4$ NCs. The XRD spectra in Fig. S-4 in the ESM show that all the three $NaYF_4$:(Yb,Er)/Ce NCs have the hexagonal phase. As indicated in Fig. 2, when

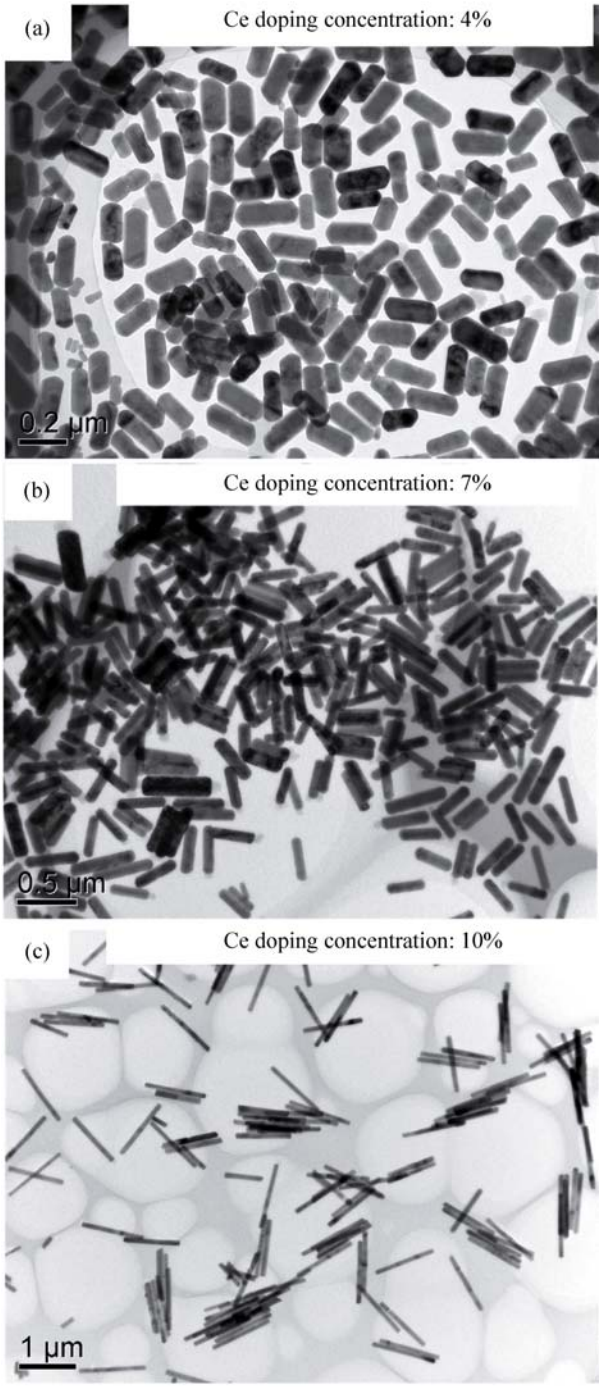

Figure 2 TEM images of $NaYF_4$:(Yb,Er)/Ce nanorods with Ce dopant concentrations of (a) 4%, (b) 7%, and (c) 10%. All the samples were synthesized with a reaction time of 24 h, and had the same doping concentrations of Yb (20%) and Er (5%)

the Ce doping concentration increased from 4% to 10%, the lengths of the hexagonal $NaYF_4$:(Yb,Er)/Ce nanorods increased from 200 to 1100 nm, while their diameters slightly decreased from 85 to 76 nm. The results indicate that the Ce doping concentration greatly influences the $NaYF_4$ crystal growth rate along the *c*-axis, probably because the RE elements with different ionic radius have greatly different interaction behavior with F^- and PEI molecules. As is well-known, such anisotropic crystal growth can also activate the cubic-to-hexagonal phase transition of $NaYF_4$ NCs [32]. We noted that if different doping concentrations of Yb or Er were used, the shape and phase of the $NaYF_4$:(Yb,Er)/Ce NCs were almost unchanged. The above results suggest that the Ce dopants can be further used to regulate the aspect ratio of the $NaYF_4$ nanorods over a broad size range, and such ability can also be found for La. Very recently, van Veggel et al. observed a similar doping effect in GdF_3:La NCs. In their study, it was found that 15% La could induce a complete orthorhombic to trigonal phase transition of the GdF_3:La NCs, however, the shape and size of the crystals were almost the same as the undoped GdF_3 NCs [48].

More interestingly, the doping effect on the anisotropic crystal growth is also suitable for other $NaREF_4$ host materials in our reaction system. Typical results for $NaGdF_4$:Ce NCs are shown in Fig. S-5 in the ESM. It was found that although both the undoped and Ce doped $NaGdF_4$ adopt the hexagonal phase, the $NaGdF_4$:5%Ce nanorods are much longer than that of the undoped $NaGdF_4$ nanorods. The results further confirm that dopants with larger ionic radius can accelerate the anisotropic crystal growth of $NaREF_4$, forming nanorods with increased aspect ratio.

2.3 Surface properties

As a result of the doping effect, we did not need a special hydrophobic surfactant in order to induce anisotropic crystal growth. Thus, the PEI surfactant was used to both stabilize the reaction process and control the particle surface properties. Two strong bands at around 3480 and 1650 cm^{-1} in the FTIR spectrum (Fig. 3) of the nanorods can be attributed to OH stretching vibrations of surface hydroxyl groups, which render the nanorods water-soluble. The effect

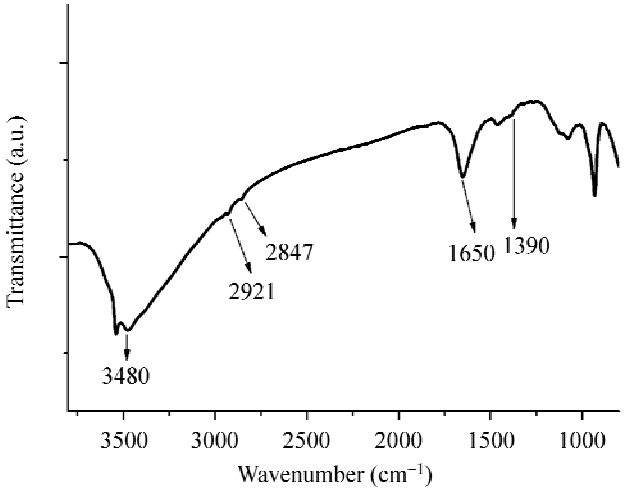

Figure 3 Typical FTIR spectrum of the synthesized nanorods

of PEI on the particle surface is further demonstrated by the presence of absorption bands from internal vibration of the amide bonds (~1390 cm^{-1}) and CH_2 stretching vibrations (2847 and 2921 cm^{-1}) in the spectrum. These PEI-coated NCs may provide a platform for direct surface functionalization of biomolecules by bioconjugate chemistry [40].

2.4 Synthesis of small hexagonal nanorods with enhanced upconversion fluorescence

The sizes of the Ce or La doped hexagonal $NaYF_4$ NCs could be further decreased by shortening the reaction time. Figures 4(a) and 4(b) show the TEM images of $NaYF_4$:(Yb,Er)/La (Y:Yb:Er:La = 70:20:5:5) and $NaYF_4$:(Yb,Er)/Ce (Y:Yb:Er:Ce = 70:20:5:5) NCs with a reaction time of 2 h. It was found that both the $NaYF_4$:(Yb,Er)/La and $NaYF_4$:(Yb,Er)/Ce NCs formed small hexagonal nanorods with lengths less than 50 nm (the XRD spectra, and energy-dispersive X-ray (EDAX) analysis are shown in Fig. S-6 in the ESM). Figure 4(c) shows the emission spectra of these two nanorods, when excited with a 975 nm 200 mW/cm^2 CW laser. The nanorods display two emission bands, which can be assigned to the 4f–4f transitions of Er^{3+} ions. The green emission originating from the $^2H_{11/2}$, $^4S_{3/2} \rightarrow {}^4I_{15/2}$ transition is observed at ~550 nm, while the red luminescence at ~660 nm is attributed to the $^4F_{9/2} \rightarrow {}^4I_{15/2}$ transition. Furthermore, as shown in Fig. 4(c), it was found that when the hexagonal $NaYF_4$:(Yb,Er)/La and $NaYF_4$:(Yb,Er)/Ce nanorods were dispersed in water, they

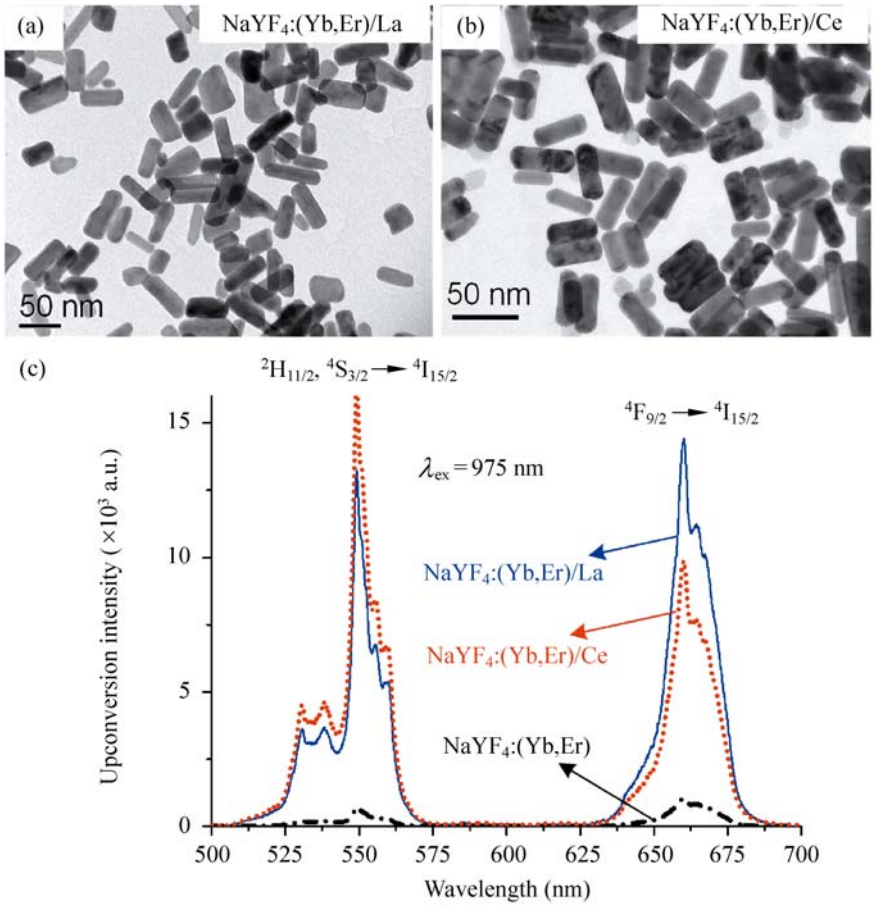

Figure 4 TEM images of (a) $NaYF_4$:(Yb,Er)/La and (b) $NaYF_4$:(Yb,Er)/Ce nanorods synthesized with a reaction time of 2 h. (c) Upconversion emission spectra of $NaYF_4$:(Yb,Er)/La, $NaYF_4$:(Yb,Er)/Ce nanorods, and $NaYF_4$:(Yb,Er) nanospheres ($d \approx 50$ nm) under 975 nm CW laser excitation with a power of 200 mW/cm^2 CW. The samples were all dispersed in water with the same concentration (1.0 wt%)

exhibited much stronger upconversion fluorescence than that of the cubic $NaYF_4$:(Yb,Er) nanospheres with the same concentration of 1.0 wt%. We note that since the undoped hexagonal $NaYF_4$ cannot be prepared, we still do not know whether our doped hexagonal $NaYF_4$ is as good as the hypothetical undoped hexagonal $NaYF_4$ for supporting upconversion fluorescence. Despite this, the dopant-controlled strategy established here can provide an alternative method to prepare hexagonal $NaYF_4$ NCs, in which the doped Yb, Er, and Ce/La ions act as sensitizers, emitters, and phase controllers, respectively. Particularly, the small size (less than 50 nm in length) of these nanorods provides the possibility to use them as probes for bioimaging *in vivo*.

2.5 Multicolor bioimaging *in vivo*

In vivo multicolor imaging is one of the most promising areas of optical bioimaging due to the potential applications in 3-D detection [50]. The hexagonal $NaYF_4$:(Yb,Er)/La nanorods ($d \approx 20$ nm, $l \approx 50$ nm) were employed as the probes for deep tissue imaging due to their suitable particle size, greatly improved upconversion fluorescence, and appropriate emission green-to-red ratio (GRR). For a typical animal study, the $NaYF_4$:(Yb,Er)/La nanorods (100 μL of a mixture with 1.0 mg/mL) were injected intramuscularly into one leg of a nude mouse. The upconversion image was taken after the injected probes became adequately dispersed into the tissues, and a defocused 975 nm 200 mW/cm^2 CW laser was used as excitation. As indicated in Fig. 5, the resulting high contrast multicolor image clearly demonstrates the feasibility of distinguishing the injected nanorods just by using the naked eye. It is interesting that the observed output color is depth-sensitive in the leg tissues because the emitted red light has much deeper tissue penetration than the green light [51]. Compared with the color-bar (left, Fig. 5) obtained from the tissue penetration test *in vitro* (see Fig. S-7 in the ESM), the observed output color approximately indicates the depth of the nanorods in the leg tissues. The emission spectra and GRR values of five selected spots in the leg (right, Fig. 5) also demonstrate the color-indicated depth regions. These results suggest a novel 3-D detection method based on the high contrast image with the color-indicated spatial resolution. In a

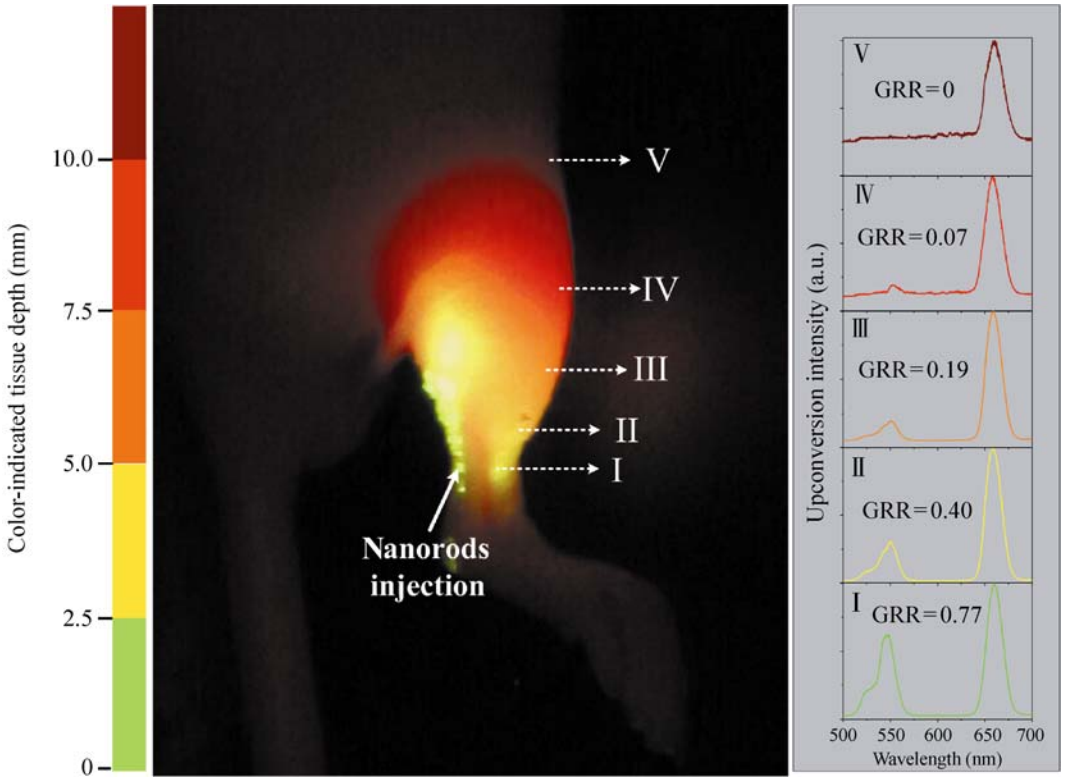

Figure 5 *In vivo* multicolor upconversion fluorescence imaging of the leg in a mouse after being injected intramuscularly with 100 μL of 1.0 mg/mL $NaYF_4$:(Yb,Er)/La nanorods, under defocused 975 nm 200 mW/cm^2 CW laser excitation. The color-bar (left) was obtained from the inset table of Fig. S-7 in the ESM. The emission spectra (right) were recorded at the indicated five spots (Ⅰ to Ⅴ) in the leg with focused 975 nm laser excitation (~1.0 W/cm^2), and the emission GRR values were calculated

clinical setting, this method may particularly suitable for pathologic location and dynamic imaging. We note that this represents the first demonstration of *in vivo* multicolor imaging by using upconversion phosphors, and furthermore our animal studies do not need expensive pulsed lasers or complicated imaging systems (see Fig. S-8 in the ESM for a description of our imager system). After *in vivo* experiments, no toxicity or other physiological complications were observed for the animal for at least 24 h after the nanorods injection (their cytotoxicity test is shown in Fig. S-9 in the ESM).

3. Conclusions

We have studied the RE doping effect on the cubic-to-hexagonal phase transition of $NaYF_4$ NCs, and established a dopant-controlled strategy for the direct synthesis of water-soluble hexagonal $NaYF_4$:RE nanorods with controllable size and improved upconversion fluorescence. Furthermore, by using the fabricated $NaYF_4$:(Yb,Er)/La small nanorods as probes, we have successfully demonstrated depth-sensitive multicolor imaging *in vivo*. We believe that the findings in this work will facilitate the design, fabrication, and functionalization of RE fluoride NCs for future innovations in bioimaging, sensors, and optical display as well as many other areas arising from these remarkable characteristics.

Acknowledgements

The authors thank the Natural Science Foundation of China (Nos. 10534030, 10904119), the National Program on Key Science Research (No. 2006CB921500), and the China Postdoctoral Science Foundation (No. 20090451076) for support.

Electronic Supplementary Material: Supplementary XRD, TEM, and EDAX results, tissue penetration tests,

description of the imager system, and cytotoxicity tests are available in the online version of this article at http://dx.doi.org/10.1007/10.1007/s12274-010-1008-2 and are accessible free of charge

References

[1] Law, M.; Sirbuly, D. J.; Johnson, J. C.; Goldberger, J.; Saykally, R. J.; Yang, P. D. Nanoribbon waveguides for subwavelength photonics integration. *Science* **2004**, *305*, 1269–1273.

[2] Cao, J.; Wang, Q.; Dai, H. Electron transport in very clean, as-grown suspended carbon nanotubes. *Nat. Mater.* **2005**, *4*, 745–749.

[3] Gur, I.; Fromer, N. A.; Geier, M. L.; Alivisatos, A. P. Air-stable all-inorganic nanocrystal solar cells processed from solution. *Science* **2005**, *310*, 462–465.

[4] Cui, Y.; Wei, Q. Q.; Park, H. K.; Lieber, C. M. Nanowire nanosensors for highly sensitive and selective detection of biological and chemical species. *Science* **2001**, *293*, 1289–1292.

[5] Stone, J. W.; Sisco, P. N.; Goldsmith, E. C.; Baxter, S. C.; Murphy, C. J. Using gold nanorods to probe cell-induced collagen deformation. *Nano Lett.* **2007**, *7*, 116–119.

[6] Peng, X.; Manna, L.; Yang, W. D.; Wickham, J.; Scher, E.; Kadavanich, A.; Alivisatos, A. P. Shape control of CdSe nanocrystals. *Nature* **2000**, *404*, 59–61.

[7] Jana, N. R.; Gearheart, L.; Murphy, C. J. Seed-mediated growth approach for shape-controlled synthesis of spheroidal and rod-like gold nanoparticles using a surfactant template. *Adv. Mater.* **2001**, *13*, 1389–1393.

[8] Sun, Y. G.; Gates, B.; Mayers, B.; Xia, Y. N. Crystalline silver nanowires by soft solution processing. *Nano Lett.* **2002**, *2*, 165–168.

[9] Wang, D. S.; Xie, T.; Li. Y. D. Nanocrystals: Solution-based synthesis and applications as nanocatalysts. *Nano Res.* **2009**, *2*, 30–46.

[10] Wang, X.; Zhuang, J.; Peng, Q.; Li, Y. D. A general strategy for nanocrystal synthesis. *Nature* **2005**, *437*, 121–124.

[11] Cao, Y. C. Synthesis of square gadolinium-oxide nanoplates. *J. Am. Chem. Soc.* **2004**, *126*, 7456–7457.

[12] Le Masne de Chermont, Q.; Chanéac, C.; Seguin, J.; Pellé, F.; Maîtrejean, S.; Jolivet, J. -P.; Gourier, D.; Bessodes, M.; Scherman, D. Nanoprobes with near-infrared persistent luminescence for *in vivo* imaging. *Proc. Natl. Acad. Sci. USA* **2007**, *104*, 9266–9271.

[13] Kömpe, K.; Borchert, H.; Storz, J.; Lobo, A.; Adam, S.; Möller, T.; Haase, M. Green-emitting $CePO_4$:Th/$LaPO_4$ core-shell nanoparticles with 70% photoluminescence quantum yield. *Angew. Chem. Int. Ed.* **2003**, *42*, 5513–5516.

[14] Stouwdam, J. W.; van Veggel, F. C. J. M. Near-infrared emission of redispersible Er^{3+}, Nd^{3+}, and Ho^{3+} doped LaF_3 nanoparticles. *Nano Lett.* **2002**, *2*, 733–737.

[15] Yu, X. F.; Chen, L. D.; Li, M.; Xie, M. Y.; Zhou, L.; Li, Y.; Wang, Q. Q. Highly efficient fluorescence of NdF_3/SiO_2 core/shell nanoparticles and the applications for *in vivo* NIR detection. *Adv. Mater.* **2008**, *20*, 4118–4123.

[16] Riwotzki, K.; Haase, M. Wet-chemical synthesis of doped colloidal nanoparticles: YVO_4:Ln (Ln = Eu, Sm, Dy). *J. Phys. Chem. B* **1998**, *102*, 10129–10135.

[17] Zhang, F.; Wan, Y. ; Yu, T.; Zhang, F. Q.; Shi, Y. F.; Xie, S. H.; Li, Y. G.; Xu, L.; Tu, B.; Zhao, D. Y. Uniform nanostructured arrays of sodium rare-earth fluorides for highly efficient multicolor upconversion luminescence. *Angew. Chem. Int. Ed.* **2007**, *46*, 7976–7979.

[18] Ehlert, O.; Thomann, R.; Darbandi, M.; Nann, T. A four-color colloidal multiplexing nanoparticle system. *ACS Nano* **2008**, *2*, 120–124.

[19] Gao, L.; Ge, X.; Chai, Z. L.; Xu, G. H.; Wang, X.; Wang. C. Shape-controlled synthesis of octahedral α-$NaYF_4$ and its rare earth doped submicrometer particles in acetic acid. *Nano Res.* **2009**, *2*, 565–574.

[20] Krämer, K. W.; Biner, D.; Frei, G.; Güdel, H. U.; Hehlen, M. P.; Lüthi, S. R. Hexagonal sodium yttrium fluoride-based green and blue emitting upconversion phosphors. *Chem. Mater.* **2004**, *16*, 1244–1251.

[21] Yi, G. S.; Lu, H. C.; Zhao, S. Y.; Yue, G.; Yang, W. J.; Chen, D. P.; Guo, L. H. Synthesis, characterization, and biological application of size-controlled nanocrystalline $NaYF_4$:Yb,Er infrared-to-visible upconversion phosphors. *Nano Lett.* **2004**, *4*, 2191–2196.

[22] Wang, L. Y.; Yan, R. X.; Huo, Z. Y.; Wang, L.; Zeng, J. H.; Bao, J.; Wang, X.; Peng, Q.; Li, Y. D. Fluorescence resonant energy transfer biosensor based on upconversion-luminescent nanoparticles. *Angew. Chem. Int. Ed.* **2005**, *44*, 6054–6057.

[23] Chatterjee, D. K.; Rufaihah, A. J.; Zhang, Y. Upconversion fluorescence imaging of cells and small animals using lanthanide doped nanocrystals. *Biomaterials* **2008**, *29*, 937–943.

[24] Nyk, M.; Kumar, R.; Ohulchanskyy, T. Y.; Bergey, E. J.; Prasad, P. N. High contrast *in vitro* and *in vivo* photoluminescence bioimaging using near infrared to near infrared up-conversion in Tm^{3+} and Yb^{3+} doped fluoride nanophosphors. *Nano Lett.* **2008**, *8*, 3834–3838.

[25] Heer, S.; Kömpe, K.; Güdel, H. U.; Haase, M. Highly efficient multicolor upconversion emission in transparent colloids of lanthanide-doped $NaYF_4$ nanocrystals. *Adv. Mater.* **2004**, *16*, 2102–2105.

[26] Zeng, J. H.; Su, J.; Li, Z. H.; Yan, R. X.; Li, Y. D. Synthesis and upconversion luminescence of hexagonal-phase $NaYF_4$:Yb, Er^{3+} phosphors of controlled size and morphology. *Adv. Mater.* **2005**, *17*, 2119–2123.

[27] Liang, X.; Wang, X.; Zhuang, J.; Peng, Q.; Li, Y. Synthesis of $NaYF_4$ nanocrystals with predictable phase and shape. *Adv. Funct. Mater.* **2007**, *17*, 2757–2765.

[28] Mai, H. X.; Zhang, Y. W.; Si, R.; Yan, Z. G.; Sun, L. D.; You, L. P.; Yan, C. H. High-quality sodium rare-earth fluoride nanocrystals: Controlled synthesis and optical properties. *J. Am. Chem. Soc.* **2006**, *128*, 6426–6436.

[29] Yi, G. S.; Chow, G. M. Synthesis of hexagonal-phase $NaYF_4$:Yb,Er and $NaYF_4$:Yb,Tm nanocrystals with efficient up-conversion fluorescence. *Adv. Funct. Mater.* **2006**, *16*, 2324–2329.

[30] Boyer, J. C.; Cuccia, L. A.; Capobianco, J. A. Synthesis of colloidal upconverting $NaYF_4$:Er^{3+}/Yb^{3+} and Tm^{3+}/Yb^{3+} monodisperse nanocrystals. *Nano Lett.* **2007**, *7*, 847–852.

[31] Wei, Y.; Lu, F. Q.; Zhang, X. R.; Chen, D. P. Synthesis of oil-dispersible hexagonal-phase and hexagonal-shaped $NaYF_4$: Yb, Er nanoplates. *Chem. Mater.* **2006**, *18*, 5733–5737.

[32] Li, C. X.; Yang, J.; Quan, Z. W.; Yang, P.; Kong, D. Y.; Lin, J. Different microstructures of β-$NaYF_4$ fabricated by hydrothermal process: Effects of pH values and fluoride sources. *Chem. Mater.* **2007**, *19*, 4933–4942.

[33] Yi, G. -S.; Chow, G. -M. Water-soluble $NaYF_4$: Yb,Er(Tm)/ $NaYF_4$/polymer core/shell/shell nanoparticles with significant enhancement of upconversion fluorescence. *Chem. Mater.* **2007**, *19*, 341–343.

[34] Shan, J.; Qin, X.; Yao, N.; Ju, Y. G. Synthesis of monodisperse hexagonal $NaYF_4$:Yb,Ln (Ln = Er, Ho and Tm) upconversion nanocrystals in TOPO. *Nanotechnology* **2007**, *18*, 445607.

[35] Li, Z. Q.; Zhang, Y. An efficient and user-friendly method for the synthesis of hexagonal-phase $NaYF_4$:Yb,Er/Tm nanocrystals with controllable shape and upconversion fluorescence. *Nanotechnology* **2008**, *19*, 345606.

[36] Wang, Y.; Tu, L. P.; Zhao, J. W.; Sun, Y. J.; Kong, X. G.; Zhang, H. Upconversion luminescence of β-$NaYF_4$: Yb^{3+}, Er^{3+}@β-$NaYF_4$ core/shell nanoparticles: Excitation power, density and surface dependence. *J. Phys. Chem. C* **2009**, *113*, 7164–7169.

[37] Abel, K. A.; Boyer, J. -C.; van Veggel, F. C. J. M. Hard proof of the $NaYF_4$/$NaGdF_4$ nanocrystal core/shell structure. *J. Am. Chem. Soc.* **2009**, *131*, 14644–14645.

[38] Li, Z. Q.; Zhang, Y. Monodisperse silica-coated polyvinylpyrrolidone/$NaYF_4$ nanocrystals with multicolor upconversion fluorescence emission. *Angew. Chem. Int. Ed.* **2006**, *45*, 7732–7735.

[39] Wang, F.; Liu, X G. Upconversion multicolor fine-tuning: Visible to near-infrared emission from lanthanide-doped $NaYF_4$ nanoparticles. *J. Am. Chem. Soc.* **2008**, *130*, 5642–5643.

[40] Wang, F.; Chatterjee, D. K.; Li, Z. Q.; Zhang, Y.; Fan, X. P.; Wang, M. Q. Synthesis of polyethylenimine/$NaYF_4$ nanoparticles with upconversion fluorescence. *Nanotechnology* **2006**, *17*, 5786–5791.

[41] Neurgaonkar, R. R.; Oliver, J. R.; Cory, W. K.; Cross, L. E.; Viehland, D. Piezoelectricity in tungsten bronze crystals. *Ferroelectrics* **1994**, *160*, 265–276.

[42] Jung, Y. -S.; Na, E. -S.; Paik, U.; Lee, J.; Kim, J. A. Study on the phase transition and characteristics of rare earth elements doped $BaTiO_3$. *Mater. Res. Bull.* **2002**, *37*, 1633–1640.

[43] Mansuy, C.; Leroux, F.; Mahiou, R.; Nedelec, J. M. Preferential site substitution in sol-gel derived Eu^{3+} doped Lu_2SiO_5: A combined study by X-ray absorption and luminescence spectroscopies. *J. Mater. Chem.* **2005**, *15*, 4129–4135.

[44] Nedelec, J. -M.; Courtheoux, L.; Jallot, E.; Kinowski, C.; Lao, J.; Laquerriere, P.; Mansuy, C.; Renaudin, G.; Turrell, S. Materials doping through sol–gel chemistry: A little something can make a big difference. *J. Sol–Gel Sci. Technol.* **2008**, *46*, 259–271.

[45] Walha, I.; Ehrenberg, H.; Fuess, H.; Cheikhrouhou, A. Structure and magnetic properties of lanthanum and calcium-deficient $La_{0.5}Ca_{0.5}MnO_3$ manganites. *J. Alloy Compd.* **2007**, *433*, 63–67.

[46] Ezekwenna, P. C.; Marasinghe, G. K.; Nam, J. -H.; James, W. J.; Yelon, W. B.; Ellouse, M.; I'Héritier, Ph. A Magnetic and crystallographic study of $(Sm/Gd)_2(Fe/Si)_{17}C_z$ solid solutions. *J. Appl. Phys.* **2000**, *87*, 6716–6718.

[47] Brixner, L. H.; Crawford, M. K.; Hyatt, G.; Carnall, W. T.; Blasse, G. Structure and luminescence of the $La_{1-x}Gd_xF_3$ system. *J. Electrochem. Soc.* **1991**, *138*, 313–317.

[48] Dong, C. H.; Raudsepp, M.; van Veggel, F. C. J. M. Kinetically determined crystal structures of undoped and La^{3+}-doped LnF_3. *J. Phys. Chem. C* **2009**, *113*, 472–478.

[49] Chen, Y. F.; Kim, M.; Lian, G.; Johnson, M. B.; Peng, X. G. Side reactions in controlling the quality, yield, and stability of high quality colloidal nanocrystals. *J. Am. Chem. Soc.* **2005**, *127*, 13331–13337.

[50] Andresen, M.; Stiel, A. C.; Fölling, J.; Wenzel, D.; Schönle, A.; Egner, A.; Eggeling, C.; Hell, S. W.; Jakobs, S. Photoswitchable fluorescent proteins enable monochromatic multilabel imaging and dual color fluorescence nanoscopy. *Nat. Biotechnol.* **2008**, *26*, 1035–1040.

[51] König, K. Multiphoton microscopy in life sciences. *J. Microsc*. **2000**, *200*, 83–104.